Nuclear Science and Techniques (2025) 36:171
https://doi.org/10.1007/s41365-025-01760-x

Studies of track finding for long-lived particles at the Super Tau-Charm Facility

Hao Li[1] · Hang Zhou[2,3] · Jin Zhang[4] · Xing-Tao Huang[5] · Jie Yang[1] · Xiao-Cong Ai[1]

Received: 7 January 2025 / Revised: 16 March 2025 / Accepted: 24 March 2025 / Published online: 1 July 2025

Abstract
Reconstructing the trajectories of charged particles in high-energy physics experiments is a complex task, particularly for long-lived particles. At the future Super Tau-Charm Facility (STCF), such particles are expected to appear in several key benchmark physics processes. A Common Tracking Software was used to reconstruct the trajectories of long-lived particles, revealing that the track-finding performance of the widely used combinatorial Kalman filter is limited by its seeding algorithm. This limitation can be mitigated by guiding the combinatorial Kalman filter using initial tracks provided by the Hough transform. The track-finding performance of the combined Hough transform and combinatorial Kalman filter was evaluated using the process $J/\psi \to \Lambda(\to p\pi^-)\bar{\Lambda}(\to \bar{p}\pi^+)$ at STCF.

Keywords Track finding · A Common Tracking Software · Hough transform · Long-lived particles

1 Introduction

Standard model (SM) [1, 2] of particle physics, including the unified electroweak (EW) and quantum chromodynamics (QCD) theories, has successfully explained nearly all experimental results in the microscopic world. However, several open questions remain, such as the baryon asymmetry of the universe, dark matter, neutrino masses, and the number of fermion flavors.

The Beijing Electron-Positron Collider II (BEPCII) and the Beijing Spectrometer (BESIII) [3] constitute the only multi-GeV e^+e^- collider operating in the τ-charm sector, offering a unique platform for studying non-perturbative QCD and strong interactions within the SM. The Super Tau-Charm Facility (STCF) [4, 5] is designed to continue and extend the physics program of BEPCII in the near future. Its goals include probing the nature of strong interactions and hadron structure, conducting precise tests of electroweak theory, exploring matter–antimatter asymmetry, and searching for physics beyond the SM.

STCF will operate at a center-of-mass energy of 2-7 GeV with a peak luminosity exceeding $0.5 \times 10^{35}\ \mathrm{cm}^{-2}\ \mathrm{s}^{-1}$ [6], which is two orders of magnitude higher than that of BEPCII. The reconstruction of charged particles is a fundamental step in the data processing pipeline of high-energy physics (HEP) experiments. To fulfill the physics goals and maximize the physics potential at STCF, charged particles must be reconstructed with high efficiency. This includes not only promptly decaying particles but also long-lived particles, such as the Λ and Ξ hyperons, which are relevant to several key physics goals at STCF.

For instance, the weak decays of Λ and Ξ hyperons provide promising channels for searching for new sources of CP violation [7–9]. Additionally, hyperon samples at STCF can be used to measure time-like nucleon and

This work was supported by the National Natural Science Foundation of China (Nos. 12375194, 12341504, 12375197, 12025502).

✉ Xiao-Cong Ai
xiaocongai@zzu.edu.cn

[1] School of Physics, Zhengzhou University, Zhengzhou 450001, China

[2] State Key Laboratory of Particle Detection and Electronics, University of Science and Technology of China, Hefei 230026, China

[3] Department of Modern Physics, University of Science and Technology of China, Hefei 230026, China

[4] School of Science, Shenzhen Campus of Sun Yat-sen University, Shenzhen 518107, China

[5] Institute of Frontier and Interdisciplinary Science, Shandong University, Qingdao 266327, China

hyperon form factors for Q^2 values up to 40 GeV^2 [5]. However, reconstructing the trajectories of long-lived particle decay products is challenging, as these particles may decay inside or outside the inner tracker, resulting in a limited number of hits recorded.

The Kalman filter (KF) [10] algorithm is commonly used for tracking in HEP and nuclear physics [11]. The combinatorial Kalman filter (CKF) [12, 13] is an extended version of the KF, in which measurements are progressively added during track propagation, guided by an initial estimate of the track parameters (the seed). The CKF accounts for magnetic field effects and material interactions during propagation, thereby enabling it to resolve hit ambiguities in high-density tracking environments. Consequently, CKF has been deployed in experiments such as ATLAS [14] and CMS [15], where thousands of tracks may be present in a single event. It also served as the primary track-finding algorithm in the Belle II experiment [16]. More recently, the CKF algorithm developed at Belle II has been adapted [17] to study tracking performance at the Circular Electron-Positron Collider (CEPC) [18].

Despite its advantages, a known limitation of KF-based tracking algorithms is their dependence on the quality of the seeding algorithm, which may result in reduced performance for long-lived particles. A track-finding algorithm based on the Hough transform, previously used in the Belle II [19] and BESIII experiments [20], was recently developed for STCF [21]. Its performance has been studied primarily for prompt particles without vertex displacement, showing promising results and strong robustness against local hit inefficiencies. However, tracking efficiency at low transverse momentum may deteriorate in the presence of background hits.

The A Common Tracking Software (ACTS) [22, 23] is an emerging open-source toolkit for HEP and nuclear physics experiments. It offers detector-agnostic, framework-independent, modular algorithms for track and vertex reconstruction. The strong performance of KF and CKF algorithms within ACTS has been demonstrated through their adoption in experiments such as FASER [24], sPHENIX [25], and several R&D projects at STCF [26] and BESIII [27]. Notably, ACTS has shown general applicability across various types of tracking detectors [28]. However, its performance in reconstructing long-lived particles has not yet been studied in detail.

In this study, we evaluate the tracking performance at STCF using a fully gaseous tracking system comprising a μ-RWELL [29]-based inner tracker and a drift chamber. We investigate the combination of the Hough transform and the ACTS CKF to enhance track finding for long-lived particles.

The remainder of this paper is organized as follows. Section 2 provides a brief overview of the STCF detector. Section 3 introduces the tracking workflows using different algorithms. Section 4 presents the tracking performance for a benchmark process involving long-lived particles at STCF. Section 5 offers concluding remarks.

2 STCF detector

The STCF detector [5] provides comprehensive coverage of the solid angle surrounding the collision point, as illustrated in Fig. 1. It consists of a tracking system composed of an Inner Tracker (ITK) and a Main Drift Chamber (MDC), along with a ring-imaging Cherenkov (RICH) detector [30] and a DIRC-like Time-of-Flight (DTOF) detector [31] for particle identification in both the barrel and endcap regions. Additionally, the detector includes a homogeneous electromagnetic calorimeter (EMC) [32], a superconducting solenoid magnet generating a 1 Tesla axial magnetic field, and a Muon Detector (MUD) positioned at the outermost layer of the system.

To ensure optimal tracking efficiency for low-momentum charged particles, the ITK covers a polar angle range of 20° to 160° (i.e., $|\cos\theta| < 0.94$) and consists of three layers of low-material-budget silicon or gaseous detectors, using either MAPS- or μ-RWELL-based technology [29]. This study focuses on the μ-RWELL-based ITK, where the three layers are placed at inner radii of 60, 110, and 160 mm, respectively. Each layer has a thickness of approximately 6.5 mm and provides a spatial resolution of about 100 µm in the r-ϕ direction and approximately 400 µm in the z-direction.

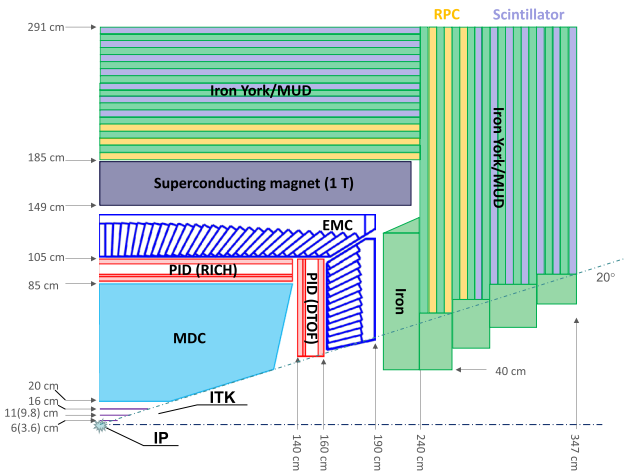

Fig. 1 (Color online) Schematic of the STCF detector. The numbers in brackets indicate the radii of the MAPS-based ITK. This figure is adapted from Ref. [5]

For the MAPS-based ITK, the radii of the three silicon layers are 36, 98, and 160 mm, respectively, and a hit resolution of 30 μm × 180 μm is assumed. Unless otherwise specified, ITK refers to the μ-RWELL-based configuration by default.

At the core of the STCF tracking system, the Main Drift Chamber (MDC) operates with a He/C_3H_8(60/40) gas mixture and features a square-cell structure with a superlayer-wire arrangement. The superlayers alternate between stereo layers ("U" or "V") and axial layers, each composed of six layers. The MDC consists of eight superlayers in the configuration AUVAUVAA, totaling 48 layers, with inner and outer radii of 200 mm and 850 mm, respectively. It provides spatial resolutions ranging from 120 μm to 130 μm.

3 Track reconstruction using combined Hough transform and CKF

The workflow for track reconstruction using the combined Hough transform and ACTS CKF is illustrated in Fig. 2. The ACTS CKF is used to identify track candidates by performing track fitting, guided by initial track parameters provided by either the ACTS seeding algorithm or the Hough transform algorithm developed within the STCF offline software.

3.1 Interface between STCF offline software and ACTS

The offline software system of the Super Tau-Charm Facility (OSCAR) [33, 34] serves as the event-processing framework for STCF. It provides core services for data handling and a suite of application tools for event generation, simulation, reconstruction, and physics analysis. For simulation, τ-charm physics processes generated by KKMC [35] are incorporated into OSCAR, and particle decays are modeled with EvtGen, as used in the BESIII experiment [36]—both integrated into the framework.

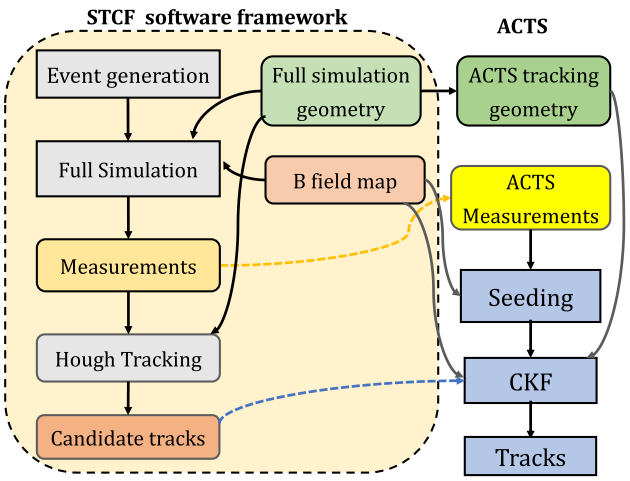

Fig. 2 Workflow for evaluating tracking performance using the STCF software framework and ACTS

The STCF detector geometry is defined using the Detector Description Toolkit (DD4hep) [37], with geometric parameters stored in compact XML [38] files. To comprehensively simulate particle interactions with the detector, Geant4 [39] is integrated into OSCAR for full simulation. A track-finding algorithm based on the Hough transform was developed for use within OSCAR.

The interface between OSCAR and ACTS enables conversion of experimental geometry, measurements, and initial track estimates into ACTS-compatible representations. Geometry plugins in ACTS facilitate this conversion from DD4hep or TGeo [40] formats into ACTS's internal geometry description. For the ITK, the readout units in each μ-RWELL layer are converted into sensitive cylindrical surfaces. For the MDC, each sense wire in a drift cell is transformed into a line surface.

Dedicated material mapping tools within ACTS are employed to project detailed material properties onto auxiliary internal surfaces of the ACTS geometry. Two ROOT [41]-based readers were developed to convert simulation data: One extracts simulated hits from the full simulation and converts them into ACTS measurements with detector resolution taken into account; the other converts the initial track parameter estimates from the Hough transform into ACTS track parameters.

3.2 ACTS seed finding

The seeding algorithm in ACTS identifies a minimal set of measurements that provide the global (x, y, z) coordinates for a particle to initiate the track-finding process. Without a seed, a track cannot be reconstructed; hence, the goal is to identify at least one seed per particle within the detector acceptance.

In a uniform magnetic field along the global z-axis, the helical trajectory of a charged particle can be accurately defined using three measurements, forming a seed. At STCF, seeds are generated by combining one compatible measurement from each of the three ITK layers, as shown in Fig. 3. For each seed candidate, the curvature and center of the projected circle on the x-y plane are determined using the Conformal Transform [42, 43]. These parameters are then used to compute the transverse momentum and transverse impact parameter, which must meet criteria optimized for relevant physics processes.

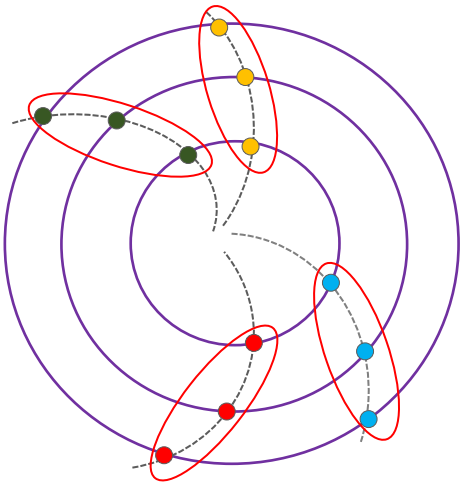

Fig. 3 Illustration of ACTS seeding using measurements from the STCF ITK

Additionally, the bending of the seed in the r-z plane must remain below a threshold optimized based on the effects of the magnetic field and multiple scattering. For further details on ACTS seeding, see Ref. [44].

3.3 Track finding with Hough transform

The principle of the Hough transform for tracking is illustrated in Fig. 4. In the presence of a magnetic field along the global z-axis, the projection of a track onto the transverse x-y plane forms a circle, while its projection onto the s-z plane (where s is the path length in the x-y plane) forms a straight line. The Conformal Transform converts the circular projection of a track that passes through the origin into a straight line in the conformal u-v space. A drift circle tangent to the projected track is also transformed into another circle tangent to the line in the u-v space.

For displaced tracks with a small but nonzero transverse impact parameter d_0 (compared with the projected track radius in the x-y plane), the trajectory of the transformed measurements (points or drift circles) in the conformal space can be approximately represented by a straight line, as shown in the middle panel of Fig. 4.

The Hough transform operates on the principle that a straight line in either the geometrical or conformal space can be described by two parameters: the angle θ of its normal and its algebraic distance ρ from the origin. A point with coordinates (u, v) on the line can be mapped to a sinusoidal curve in Hough space using:

$$\rho = u \cdot \cos\alpha + v \cdot \sin\alpha. \tag{1}$$

For a circle centered at (u, v) with radius r tangent to the line, this produces two sinusoidal curves:

$$\rho = u \cdot \cos\alpha + v \cdot \sin\alpha \pm r. \tag{2}$$

The process of identifying measurements or drift circles belonging to the same track involves finding curves in the Hough space that intersect, as shown in the right panel of Fig. 4. A 2D histogram with optimized binning (based on track parameter resolution) is filled whenever a curve passes through a bin, and peaks in the histogram are identified, as detailed in Ref. [21]. The parameters at the intersections correspond to track parameters projected in either the x-y or s-z planes.

The track-finding workflow using the Hough transform in OSCAR is illustrated in Fig. 5. First, measurements from the ITK and MDC axial wires are used to reconstruct 2D track projections in the x-y plane, followed by circle fitting to extract their parameters. These 2D tracks

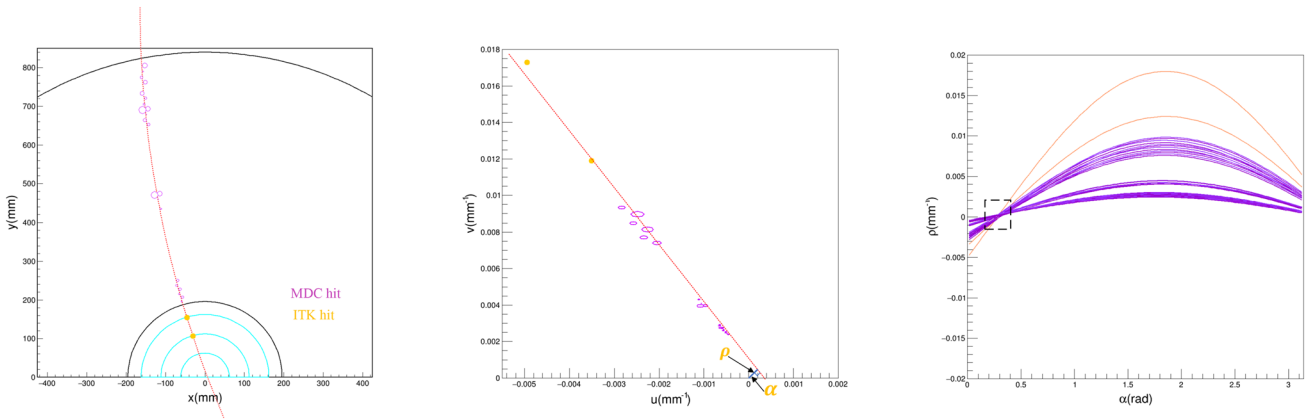

Fig. 4 (Color online) Example mapping of detector measurements in the transverse x-y plane (left) onto the Conformal u-v space (middle), and then onto Hough curves in Hough space (right), for a proton p in a $J/\psi \to \Lambda(\to p\pi^-)\bar{\Lambda}(\to \bar{p}\pi^+)$ event. The proton decays between the first and second layers of the ITK, producing two hits in ITK. Yellow and purple indicate ITK and MDC hits, respectively

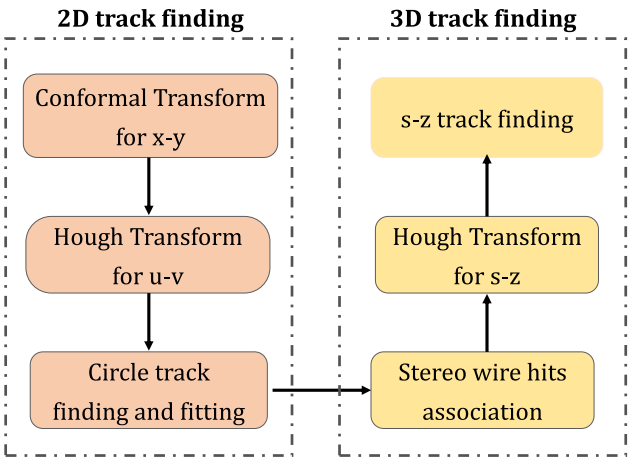

Fig. 5 Workflow for track finding using the Hough transform in OSCAR

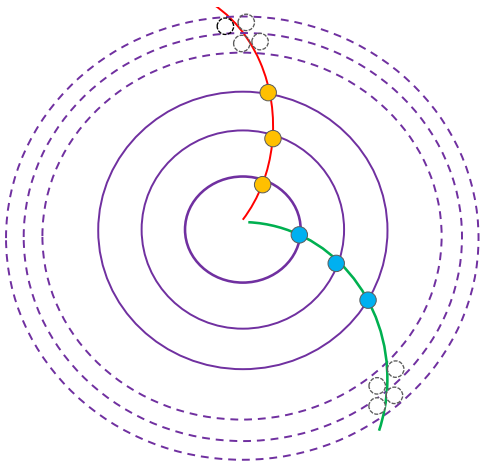

Fig. 6 Illustration of track finding using ACTS CKF with STCF ITK and MDC. Only two MDC layers are depicted

are then associated with candidate measurements from MDC stereo wires. The z-position and path length s at each stereo wire are simultaneously estimated. Since each stereo wire yields two possible z-position solutions and may include incorrectly assigned hits, a second application of the Hough transform is used to identify tracks in the s-z plane. Further details can be found in Ref. [21].

3.4 Track finding with ACTS CKF

Beginning with a set of initial track parameters, the ACTS CKF uses the ACTS track propagator to search for compatible measurements on a given surface through KF track fitting, as illustrated in Fig. 6. This iterative process, also referred to as track-following, associates the best-matching measurement with the track and updates the track parameters accordingly for continued propagation.

4 Performance studies

4.1 Monte Carlo samples

The decay process $J/\psi \to \Lambda(\to p\pi^-)\bar{\Lambda}(\to \bar{p}\pi^+)$ serves as an important benchmark channel at STCF, enabling several key physics studies related to Λ baryons. Signal events were generated using the KKMC and EvtGen generators within the OSCAR framework, without considering bream-related backgrounds, to evaluate tracking performance.

Figure 7 shows the 2D distributions of $\cos\theta$ versus p_{T}, vertex displacement in the x-y plane V_{xy} versus p_{T}, and transverse impact track parameter d_0 versus p_{T}, for protons (and anti-protons), denoted as $p(\bar{p})$, and π in $J/\psi \to \Lambda(\to p\pi^-)\bar{\Lambda}(\to \bar{p}\pi^+)$ events. The π has relatively low transverse momentum, with p_{T} below 310 MeV/c, while $p(\bar{p})$ reach up to 1.1 GeV/c.

A significant fraction of particles decay outside the first layer of the ITK. However, most reconstructed tracks have d_0 values smaller than the radius of the first ITK layer, especially for $p(\bar{p})$.

Following event generation, Geant4 was used to simulate hits from final-state particles, which originated from primary interactions and traversed the STCF tracking system under a uniform 1 T magnetic field. Detector measurements were then obtained by applying Gaussian smearing to the simulated hit positions, using zero mean and widths determined by the detector resolution.

4.2 Track-finding performance

The performance of track finding—comprising seed finding using either the ACTS seeding algorithm or the Hough transform algorithm in the first stage, and track following using ACTS CKF in the second stage—was studied.

Considering the acceptance of the STCF tracking system, only truth particles with p_{T} above 50 MeV/c and $|\cos\theta|$ below 0.94 were included in the performance evaluation. This evaluation involves identifying the primary particle [22] of a seed or a track, i.e., the simulated particle contributing the most hits to that seed or track.

The seeding process serves as the initial step in track finding using the CKF and ideally should provide seeds for all particles within the detector acceptance. The ACTS

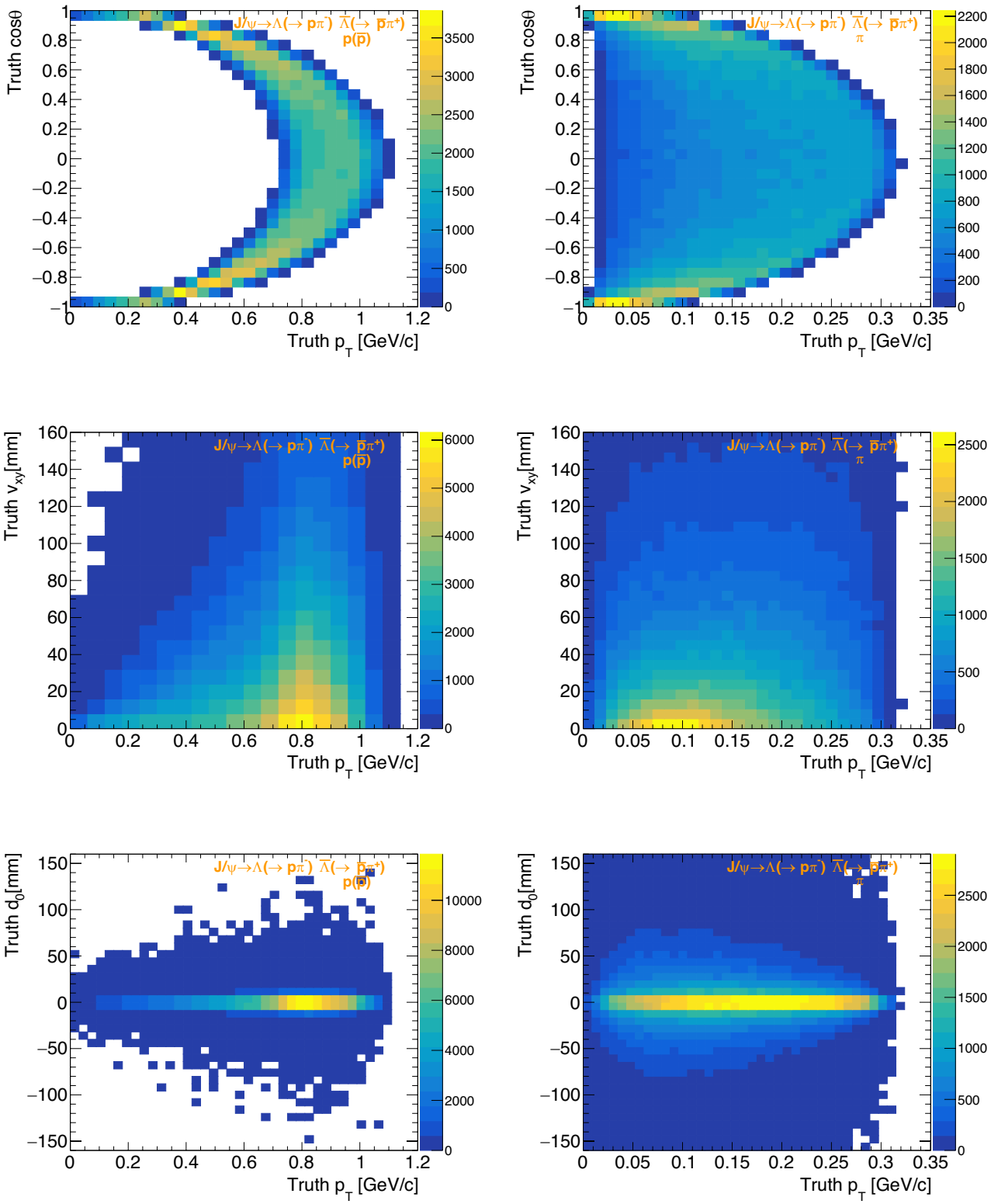

Fig. 7 (Color online) Distributions of particle cosθ versus p_{T} (top), vertex displacement in the x-y plane V_{xy} versus p_{T} (middle), and d_0 versus p_{T} (bottom) for $p(\bar{p})$ (left) and π (right) in $J/\psi \to \Lambda(\to p\pi^-)\bar{\Lambda}(\to \bar{p}\pi^+)$ events

seeding efficiency is defined as the fraction of particles within the acceptance region whose seeds are matched to hits originating from the same particle in all three ITK layers. For the Hough transform, seeding efficiency is defined as the fraction of seeds with at least 50% of hits originating from the same primary particle.

ACTS seeding is only possible for tracks from particles that produce hits in all three ITK layers, which corresponds to a vertex displacement below 66.5 mm. A comparison of the efficiencies of ACTS seeding and the Hough transform as a function of vertex displacement in the x-y plane (V_{xy}) is shown in Fig. 8 (top panels). ACTS seeding efficiency approaches 100% when there are at least three ITK measurements. In particular, ACTS seeding provides higher efficiency than the Hough transform for π with small V_{xy}. However, ACTS efficiency drops sharply to zero if fewer than three ITK hits are present, highlighting a key limitation for long-lived particles. In contrast, the Hough transform, functioning as a global tracking algorithm, shows reduced sensitivity to the number of ITK layers traversed.

Figure 8 (bottom panels) shows seeding efficiency as a function of particle p_{T}. The Hough transform achieves over 90% efficiency for $p(\bar{p})$ with p_{T} above 350 MeV/c, and over 80% for π with p_{T} above 85 MeV/c—an improvement over ACTS seeding.

Reconstructed tracks are required to have at least five measurements and reconstructed $|\cos\theta| < 0.94$. A track is matched to its primary particle if at least 50% of its hits originate from that particle (track purity). A track not matched to its primary particle is labeled as fake. If multiple tracks match the same simulated particle, the one with the highest

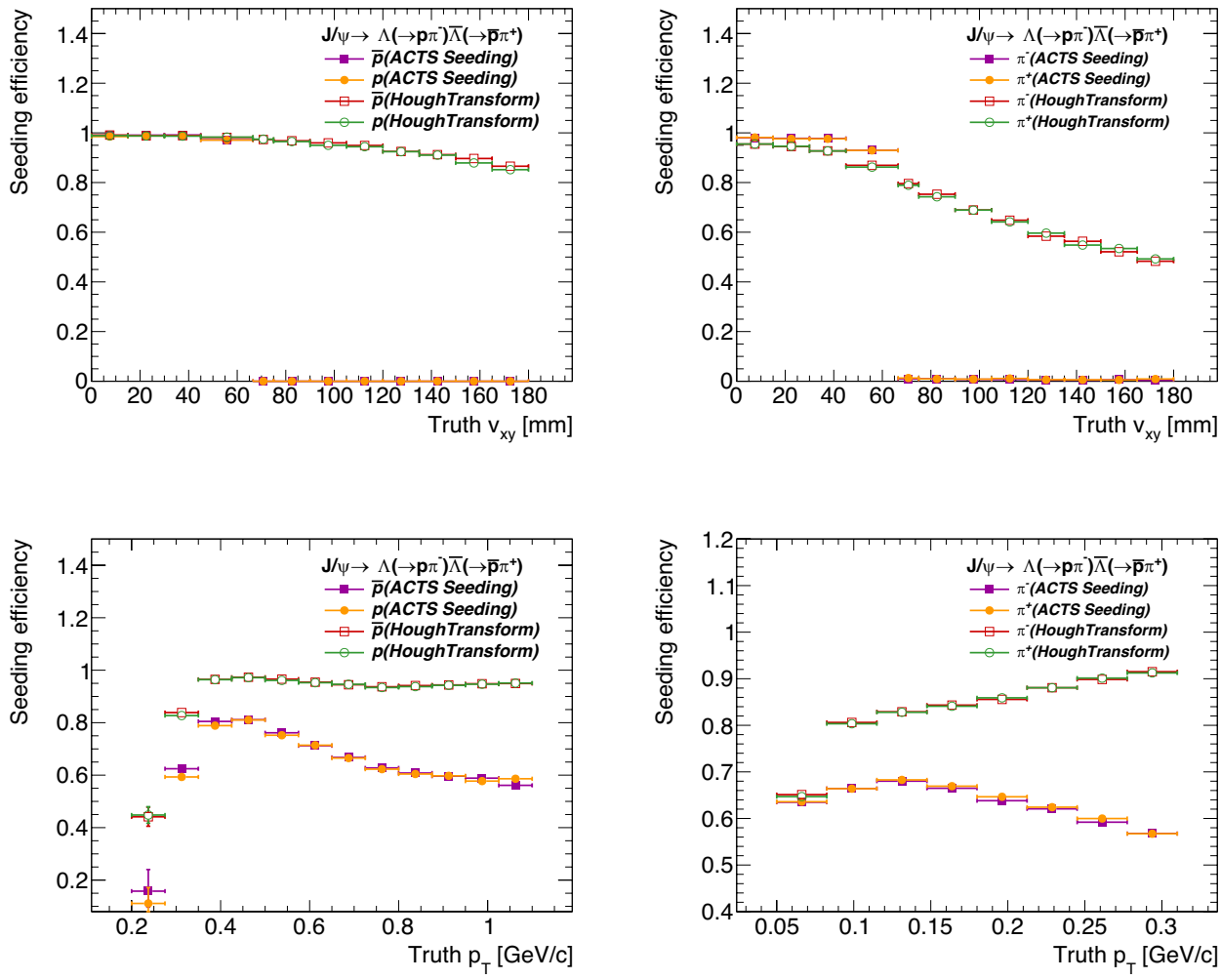

Fig. 8 Seeding efficiency vs. particle V_{xy} (top) and p_{T} (bottom) for $p(\bar{p})$ (left) and π (right) in 200k $J/\psi \to \Lambda(\to p\pi^-)\bar{\Lambda}(\to \bar{p}\pi^+)$ events. Solid purple squares and yellow dots represent the ACTS seeding for negative and positive particles, respectively. Hollow red squares and green circles represent the Hough transform for negative and positive particles, respectively

purity is considered the true track, and others are labeled as duplicates.

Track reconstruction efficiency is defined as the fraction of simulated particles (with at least five hits in the detector acceptance) that are matched to reconstructed tracks. The fake rate is the fraction of fake tracks among all reconstructed tracks. The duplication rate is the fraction of particles with at least one duplicate track among those with five or more simulated hits.

Figure 9 shows the tracking efficiency as a function of particle V_{xy} and p_{T}. As expected, tracking efficiency using ACTS seeding with CKF drops to zero when V_{xy} exceeds 66.5 mm. In contrast, tracking with the Hough transform and CKF shows weaker dependence on V_{xy}, achieving above 80% for $p(\bar{p})$ with p_{T} above 350 MeV/c and above 70% for π with p_{T} above 85 MeV/c.

Figure 10 presents the fake and duplicate rates for the two seeding strategies. The fake rate remains below 0.4%. A non-negligible number of duplicate tracks appear for particles with p_{T} below 150 MeV/c due to looping trajectories in the magnetic field. ACTS seeding yields lower fake and duplicate rates compared to Hough transform seeding.

The tracking performance of an alternative MAPS-based ITK was compared to that of a μ-RWELL-based ITK for long-lived particles. Figure 11 shows the tracking efficiency, fake rate, and duplicate rate using the combined Hough transform and ACTS CKF for both designs. Due to its smaller radii in the first two layers, the MAPS-based ITK is less effective for long-lived particles and shows slightly lower tracking efficiency than the μ-RWELL-based ITK. However, fake and duplicate rates are similar between the two designs.

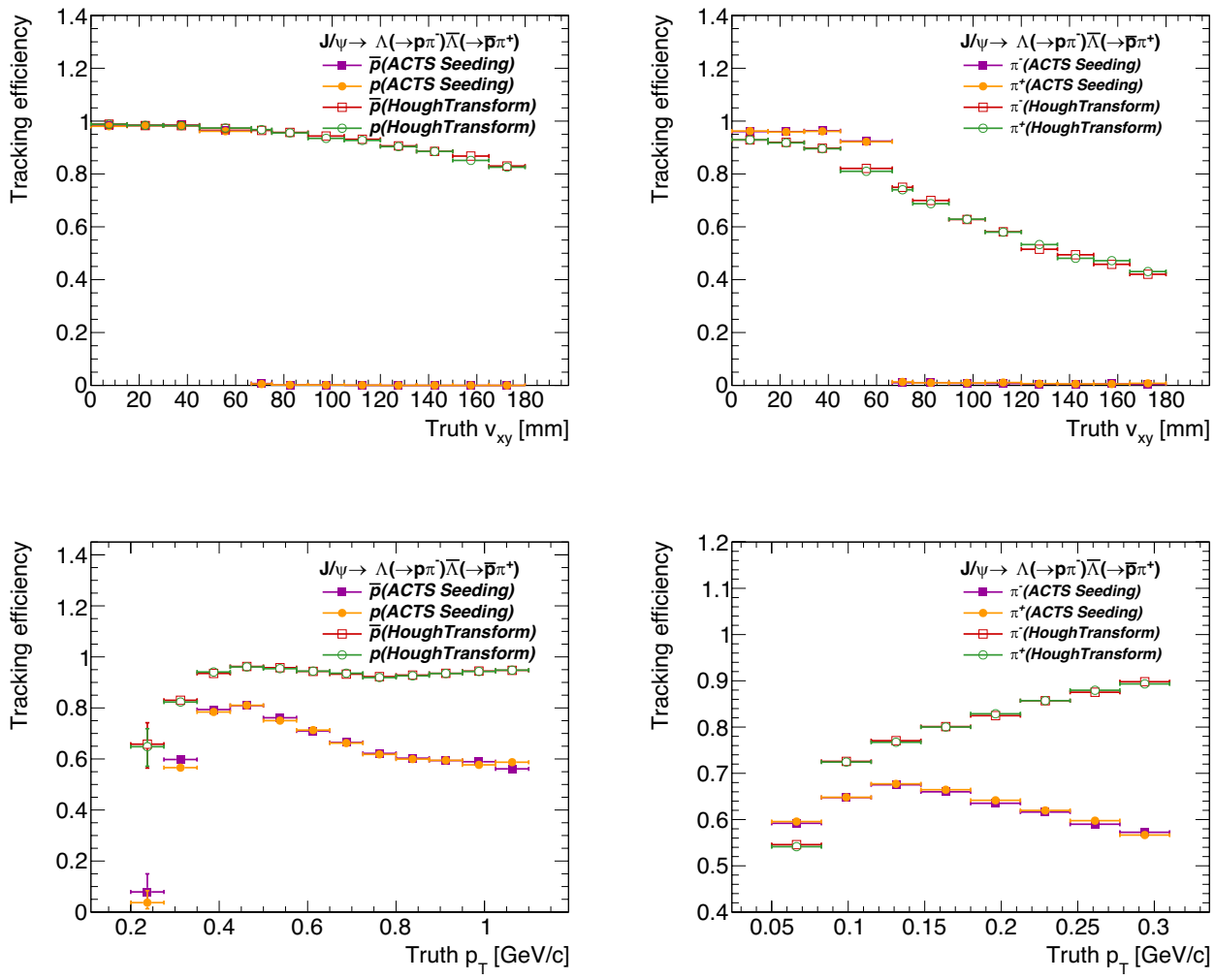

Fig. 9 Tracking efficiency vs. particle V_{xy} (top) and p_{T} (bottom) for $p(\bar{p})$ (left) and π (right) in 200k $J/\psi \to \Lambda(\to p\pi^-)\bar{\Lambda}(\to \bar{p}\pi^+)$ events. Same color and marker conventions as in Fig. 8

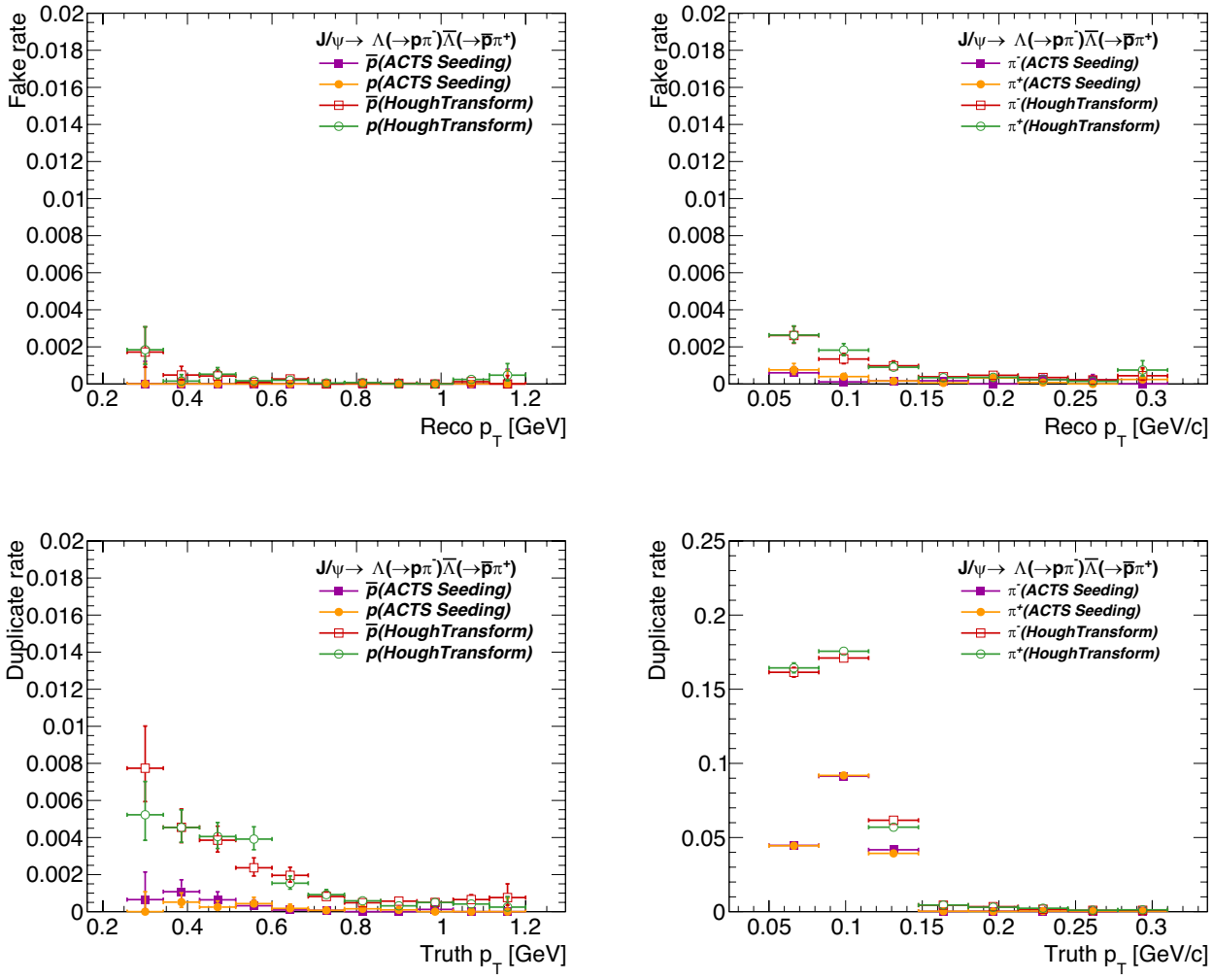

Fig. 10 Fake rate vs. track p_{T} (top) and duplicate rate vs. particle p_{T} (bottom) for $p(\bar{p})$ (left) and π (right) in 200k $J/\psi \to \Lambda(\to p\pi^-)\bar{\Lambda}(\to \bar{p}\pi^+)$ events. Same color and marker conventions as in Fig. 8

5 Conclusion

Processes involving long-lived particles offer opportunities to probe CP violation, strong interactions, and related phenomena at the future STCF. However, achieving high-performance track reconstruction for long-lived particles presents significant challenges for the STCF tracking system. The CKF is one of the most widely used track-finding algorithms in HEP experiments, and its performance is highly dependent on that of the seeding algorithm.

For long-lived particles, CKF using traditional seeding strategies—typically based on measurements from the inner detectors—exhibits considerable performance degradation. In this study, we evaluate for the first time the combined performance of the Hough transform as a seeding algorithm for the ACTS CKF within the STCF offline software framework. The performance was assessed using simulated events of $J/\psi \to \Lambda(\to p\pi^-)\bar{\Lambda}(\to \bar{p}\pi^+)$ at the STCF.

The results demonstrate that CKF seeded by the Hough transform achieves improved efficiency compared to traditional seeding approaches, particularly for particles with large vertex displacements. Specifically, tracking efficiency using the combined Hough transform and CKF reaches approximately 80% for protons and antiprotons with above 350 MeV/c and over 70% for π with p_{T} above 85 MeV/c, with negligible fake track rates. Duplicate tracks are observed mainly for particles with p_{T} below 150 MeV/c, which tend to exhibit looping trajectories.

Future enhancements, such as extending the 2D Hough space to a 3D Hough space—where track projections in

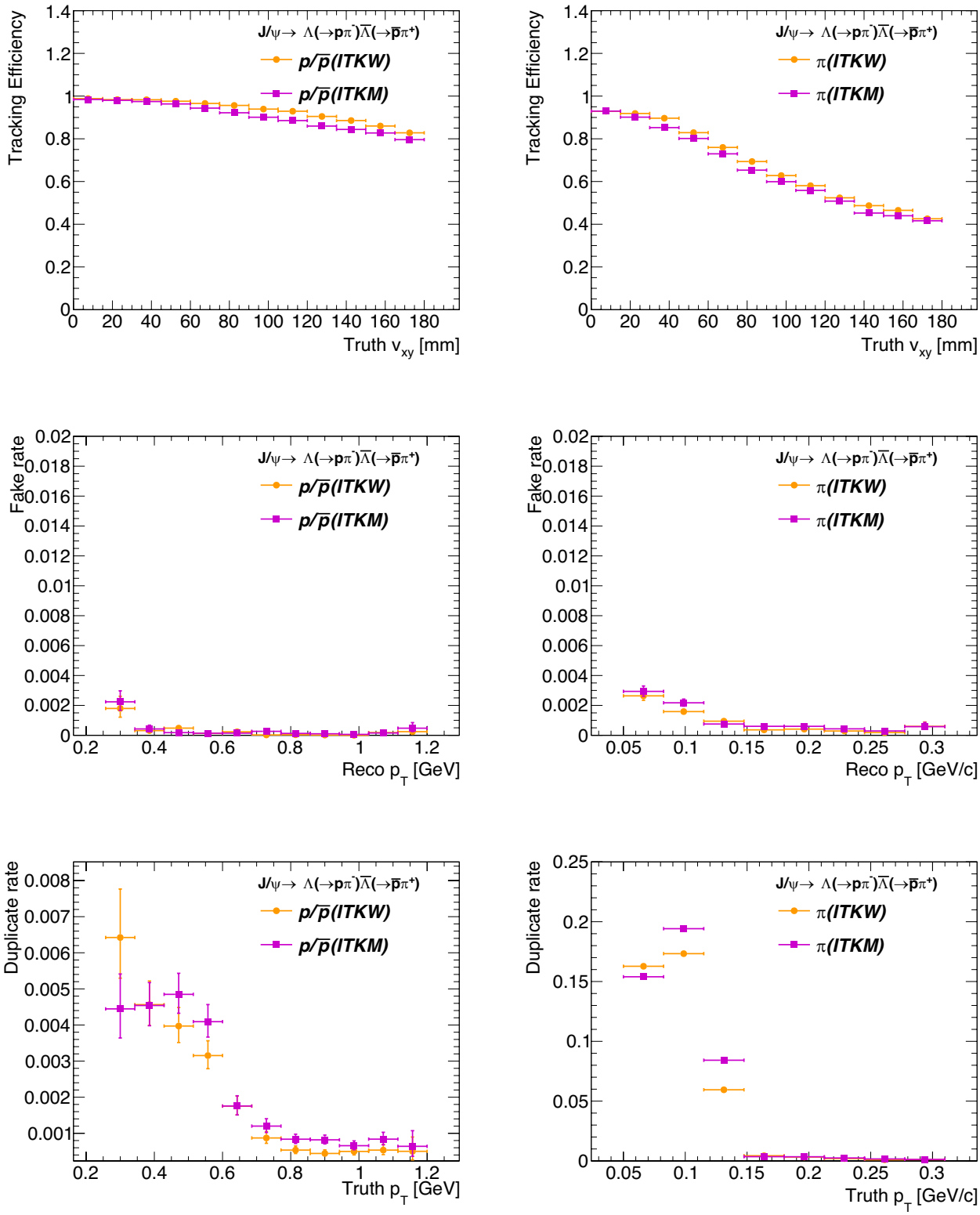

Fig. 11 Tracking efficiency (top), fake rate (middle), and duplicate rate (bottom) as a function of V_{xy} and p_T for $p(\bar{p})$ (left) and π (right) in 200k $J/\psi \to \Lambda(\to p\pi^-)\bar{\Lambda}(\to \bar{p}\pi^+)$ events, using the combined Hough transform and ACTS CKF. Yellow dots and purple squares represent results for the μ-RWELL-based ITK (ITKW) and MAPS-based ITK (ITKM), respectively

the x-y plane not passing through the origin are described using three dedicated parameters—are anticipated to further improve tracking efficiency for long-lived particles at STCF and similar facilities.

Author contributions All authors contributed to the study conception and design. Material preparation, data collection and analysis were performed by Hao Li, Hang Zhou, and Xiao-Cong Ai. The first draft of the manuscript was written by Hao Li and Xiao-Cong Ai, and all authors commented on previous versions of the manuscript. All authors read and approved the final manuscript.

Data availability The data that support the findings of this study are openly available in Science Data Bank at https://cstr.cn/31253.11.sciencedb.j00186.00719 and https://doi.org/10.57760/sciencedb.j00186.00719.

Declarations

Conflict of interest The authors declare that they have no Conflict of interest.

References

1. M.K. Gaillard, P.D. Grannis, F.J. Sciulli, The standard model of particle physics. Rev. Mod. Phys. **71**, S96–S111 (1999). https://doi.org/10.1103/RevModPhys.71.S96
2. J.F. Donoghue, E. Golowich, B.R. Holstein, *Dynamics of the Standard Model*, 2nd Edition, Cambridge Monographs on Particle Physics, Nuclear Physics and Cosmology, (Cambridge University Press, 2014). https://doi.org/10.1017/CBO9780511803512
3. M. Ablikim et al., Design and construction of the BESIII detector. Nucl. Instrum. Method Phys. Res. Sect. A **614**, 345–399 (2010). https://doi.org/10.1016/j.nima.2009.12.050
4. H. Peng, Y. Zheng, X. Zhou, Super Tau-Charm Facility of China. Physics **49**, 513–524 (2020). https://doi.org/10.7693/wl20200803
5. M. Achasov, X.C. Ai, L.P. An et al., STCF conceptual design report (Volume 1): physics & detector. Front. Phys. **19**, 14701 (2023). https://doi.org/10.1007/s11467-023-1333-z
6. L. Tao, W. Qian, L. Qing, Design of bunch length and charge monitor based on cavity resonator for injector of Super Tau-Charm Facility. Nuclear Techniques (in Chinese) **47**, 100204. https://doi.org/10.11889/j.0253-3219.2024.hjs.47.100204
7. X.G. He, H. Steger, G. Valencia, Status of CP violation in hyperon decays. Phys. Lett. B **272**, 411–418 (1991). https://doi.org/10.1016/0370-2693(91)91851-L
8. X.G. He, CP violation from supersymmetry in hyperon decays. Nucl. Phys. A **684**, 710–712 (2001). https://doi.org/10.1016/S0375-9474(01)00469-9
9. BESIII Collaboration, Polarization and entanglement in baryon–antibaryon pair production in electron–positron annihilation. Nature Physics **15**, 631–634 (2019). https://doi.org/10.1038/s41567-019-0494-8
10. R.E. Kalman, A new approach to linear filtering and prediction problems. J. Basic Eng. **82**, 35–45 (1960). https://doi.org/10.1115/1.3662552
11. X.Y. Ju, Y.H. Leung, S. Radhakrishnann et al., Applying the Kalman filter particle method to strange and open charm hadron reconstruction in the STAR experiment. Nucl. Sci. Tech. **34**, 158 (2023). https://doi.org/10.1007/s41365-023-01320-1
12. N. Braun, *Combinatorial Kalman Filter* (Springer International Publishing, Cham, 2019), pp.117–174. https://doi.org/10.1007/978-3-030-24997-7_6
13. R. Frühwirth, A. Strandlie, *Track Finding* (Springer International Publishing, Cham, 2021), pp.81–102. https://doi.org/10.1007/978-3-030-65771-0_5
14. ATLAS Collaboration, Software performance of the ATLAS track reconstruction for LHC Run 3. Computing and Software for Big Science **8**, 9 (2024). https://doi.org/10.1007/s41781-023-00111-y
15. CMS Collaboration, CMS tracking performance in Run 2 and early Run 3. Tech. Rep., CERN, Geneva (2024). https://doi.org/10.22323/1.448.0074. arXiv:2312.08017
16. V. Bertacchi, T. Bilka, N. Braun et al., Track finding at Belle-II. Comput. Phys. Commun. **259**, 107610 (2021). https://doi.org/10.1016/j.cpc.2020.107610
17. M.Y. Liu, W.D. Li, X.T. Huang et al., Simulation and reconstruction of particle trajectories in the CEPC drift chamber. Nucl. Sci. Tech. **35**, 128 (2024). https://doi.org/10.1007/s41365-024-01497-z
18. X. Lou, The circular electron positron collider. Nat. Rev. Phys. **1**, 232–234 (2019). https://doi.org/10.1038/s42254-019-0047-1
19. S. Pohl, Track reconstruction at the first level trigger of the Belle II experiment. (April 2018). https://doi.org/10.5282/edoc.22085
20. J. Zhang, Y. Zhang, H.M. Liu et al., Low transverse momentum track reconstruction based on the Hough transform for the BESIII drift chamber. Radiat. Detect. Technol. Method. **2**, 20 (2018). https://doi.org/10.1007/s41605-018-0052-4
21. H. Zhou, K. Sun, Z. Lu et al., Global track finding based on the Hough transform in the STCF detector. Nucl. Instrum. Method Phys. Res. Sect. A **1075**, 170357 (2025). https://doi.org/10.1016/j.nima.2025.170357
22. X. Ai, C. Allaire, N. Calace et al., A common tracking software project. Comput. Softw. Big Sci. **6**, 8 (2022) https://doi.org/10.1007/s41781-021-00078-8
23. A. Salzburger, P. Gessinger, F. Klimpel et al., acts-project/acts: v38.2.0. (Dec. 2024). https://doi.org/10.5281/zenodo.14502803
24. J. Liu, H. Pang, C. Wang et al., FASER experiment: an introduction and research progress. Chin. Sci. Bull. **69**, 1025–1033 (2024). https://doi.org/10.1360/TB-2023-1034
25. J.D. Osborn, A.D. Frawley, J. Huang et al., Implementation of ACTS into sPHENIX track reconstruction. Comput. Softw. Big Sci. **5**. 23 (2021). https://doi.org/10.1007/978-3-030-24997-7_6
26. X. Ai, X. Huang, Y. Liu, Implementation of ACTS for STCF track reconstruction. J. Instrum. **18**, P07026 (2023). https://doi.org/10.1088/1748-0221/18/07/P07026
27. Y. Liu, X.C. Ai, G.Y. Xiao et al., Simulation study of BESIII with stitched CMOS pixel detector using acts. Nucl. Sci. Tech. **34**, 203 (2023). https://doi.org/10.1007/s41365-023-01353-6
28. X. Ai, X. Huang, H. Li et al., Application of ACTS for gaseous tracking detectors. Mod. Phys. Lett. A **39**, 2440009 (2024). https://doi.org/10.1142/S0217732324400091
29. Y. Zhou, Y. Lv, L. Shang et al., Fabrication and performance of a μRWELL detector with diamond-Like carbon resistive electrode and two-dimensional readout. Nucl. Instrum. Method Phys. Res. Sect. A **927**, 31–36 (2019). https://doi.org/10.1016/j.nima.2019.01.036
30. P. Li, S. Chen, Q. Liu et al., Study of hybrid micropattern gaseous detector with CsI photocathode for Super Tau-Charm facility RICH. J. Instrum. **18**, P04028 (2023). https://doi.org/10.1088/1748-0221/18/04/P04028
31. B. Qi, M. Shao, J. Liu, Imaging-based likelihood analysis for the STCF DTOF detector. Nucl. Instrum. Method Phys. Res. Sect. A **1049**, 168090 (2023). https://doi.org/10.1016/j.nima.2023.168090
32. Z. Jia, H. Yu, H. Mo et al., A light yield enhancement method using wavelength shifter for the STCF EMC. Nucl. Instrum.

Method Phys. Res. Sect. A **1050**, 168173 (2023). https://doi.org/10.1016/j.nima.2023.168173
33. W. Huang, H. Li, H. Zhou et al., Design and development of the core software for STCF offline data processing. J. Instrum. **18**, P03004 (2023). https://doi.org/10.1088/1748-0221/18/03/p03004
34. X. Ai, X. Huang, T. Li et al., Design and development of STCF offline software. Mod Phys. Lett. A **39**, 2440006 (2024). https://doi.org/10.1142/S0217732324400066
35. S. Jadach, B.F.L. Ward, Z. Was, Coherent exclusive exponentiation for precision Monte Carlo calculations. Phys. Rev. D **63**, 113009 (2001). https://doi.org/10.1103/PhysRevD.63.113009
36. P. Rong-Gang, Event generators at BESIII. Chin. Phys. C **32**, 599 (2008). https://doi.org/10.1088/1674-1137/32/8/001
37. M. Frank, F. Gaede, C. Grefe et al., DD4hep: a detector description toolkit for high energy physics experiments. J. Phys. Conf. Ser. **513**, 022010 (2014). https://doi.org/10.1088/1742-6596/513/2/022010
38. T. Bray, J. Paoli, C.M. Sperberg-Mcqueen, Extensible markup language. World Wide Web J. **2**, 29–66 (1997). https://doi.org/10.1007/978-1-4302-0187-8_6
39. S. Agostinelli, J. Allison, K. Amako et al., Geant4—a simulation toolkit. Nucl. Instrum. Method Phys. Res. Sect. A **506**, 250–303 (2003). https://doi.org/10.1016/S0168-9002(03)01368-8
40. R. Brun, A. Gheata, M. Gheata, The ROOT geometry package. Nucl. Instrum. Meth. Phys. Res. Sect. A **502**, 676–680 (2003). https://doi.org/10.1016/S0168-9002(03)00541-2
41. R. Brun, F. Rademakers, ROOT — An object oriented data analysis framework. Nucl. Instrum. Meth. Phys. Res. Sect. A **389**, 81–86 (1997). https://doi.org/10.1016/S0168-9002(97)00048-X
42. M. Hansroul, H. Jeremie, D. Savard, Fast circle fit with the conformal mapping method. Nucl. Instrum. Method Phys. Res. Sect. A **270**, 498–501 (1988). https://doi.org/10.1016/0168-9002(88)90722-X
43. Q.G. Liu, S.L. Zang, W.G. Li et al., Track reconstruction using the TSF method for the BESIII main drift chamber. Chin. Phys. C **32**, 565–571 (2008). https://doi.org/10.1088/1674-1137/32/7/011
44. ACTS Seeding., https://acts.readthedocs.io/en/latest/core/reconstruction/pattern_recognition/seeding.html